Journal of Zhejiang University-SCIENCE A (Applied Physics & Engineering)
ISSN 1673-565X (Print); ISSN 1862-1775 (Online)
www.zju.edu.cn/jzus; www.springerlink.com
E-mail: jzus@zju.edu.cn

A cutterhead energy-saving technique for shield tunneling machines based on load characteristic prediction*

Xu YANG[1], Guo-fang GONG[†‡1], Hua-yong YANG[1], Lian-hui JIA[2], Qun-wei YING[3]

([1]*The State Key Lab of Fluid Power Transmission and Control, Zhejiang University, Hangzhou 310027, China*)

([2]*China Railway Engineering Equipment Group Co., Ltd., Zhengzhou 450016, China*)

([3]*Hangzhou Boiler Group Co., Ltd., Hangzhou 310021, China*)

[†]E-mail: gfgong@zju.edu.cn

Received Oct. 23, 2014; Revision accepted Apr. 17, 2015; Crosschecked Apr. 20, 2015

Abstract: In this paper, we propose a shield cutterhead load characteristic forecast method and apply it to optimize the efficiency of the cutterhead driving system. For the forecast method, wavelet transform is used for preprocessing, and grey model GM(1,1) for forecasting. The performance of the wavelet-based GM(1,1) (WGM(1,1)) is illustrated through field data based load characteristic prediction and analysis. A cutterhead mode control strategy (CMCS) is presented based on the WGM(1,1). The CMCS can not only provide operators with some useful operating information but also optimize the stator winding connection. Finally, the CMCS is tested on a cutterhead driving experimental platform. Results show that the optimized stator winding connection can improve the system efficiency through reducing the energy consumption under part-load conditions. Therefore, the energy-saving CMCS is useful and practical.

Key words: Shield cutterhead, Driving system, Load characteristic forecast, Cutterhead mode control strategy (CMCS)
doi:10.1631/jzus.A1400323 **Document code:** A **CLC number:** TH137

1 Introduction

A shield tunneling machine (STM) is a large-scale piece of equipment (Fig. 1) widely used in the construction of subways, railways, roadways, and city infrastructure (He *et al*., 2012; Liu *et al*., 2014). It can quickly, safely, and efficiently excavate and discharge soil, and install tunnel supports through its subsystems.

As one key subsystem of an STM, the shield cutterhead is responsible for cutting front rock and soil. With this heavy work, it is thus the most energy-consuming subsystem. Take a CTE6250 machine (Φ6250 mm) for example, the cutterhead installed power (945 kW) accounts for about 55% of total installed power. Therefore, it is very important to increase the efficiency of cutterhead driving system.

Fig. 2 shows a simplified diagram of the cutterhead hydraulic driving system of the CTE6250 (Xing *et al*., 2010). The hydraulic system consists mainly of three induction motors, three variable pumps, and eight variable motors. Connected in parallel, the eight motors are used to drive the cutterhead. While driving the cutterhead, the driving system wastes a lot of energy due to the combined energy losses of the induction motors and hydraulic system.

To cope with these energy losses, variable speed hydrostatic control technology has been introduced recently to cutterhead driving systems (Yang *et al*., 2010; Shi *et al*., 2014). With the high performance of fixed displacement pump at low cutterhead

‡ Corresponding author

* Project supported by the National Basic Research Program (973) of China (No. 2013CB035400), the Science Fund for Creative Research Groups of the National Natural Science Foundation of China (No. 51221004), and the National High-Tech R&D (863) Program of China (No. 2012AA041803)

ORCID: Xu YANG, https://orcid.org/0000-0001-9462-0507; Guo-fang GONG, https://orcid.org/0000-0001-9553-8783

speed, the variable speed hydrostatic control technology has achieved some increase in efficiency. Xing *et al*. (2009) proposed a pump optimized combination method to improve cutterhead efficiency.

Fig. 1 Shield tunneling machine

In this paper, we propose an energy-saving technique for cutterhead based on load characteristic prediction. Section 2 introduces a wavelet-based grey model for forecasting the cutterhead load characteristic and illustrates its performance through field data analysis. Based on this method, Section 3 proposes an energy-saving control strategy for a shield cutterhead hydraulic system. The energy-saving performance of the control strategy is evaluated by experiments in Section 4. Finally, Section 5 presents the conclusions.

2 Cutterhead load characteristic prediction

One main goal of this study was to forecast the cutterhead load characteristic of the next ring of a tunnel. Therefore, a load parameter closely related to the geological conditions is needed. For this purpose, the torque penetration index (TPI), which not only can approximately reflect the geology but also is accessible, is introduced (Song *et al*., 2007; Zhang *et al*., 2012). Based on the TPI, the average torque penetration index (ATPI) is defined to describe the cutterhead load characteristic of a certain length of tunneling:

$$P = v / \omega, \tag{1}$$

$$\mathrm{TPI} = T / P, \tag{2}$$

$$\mathrm{ATPI} = \frac{\int \mathrm{TPI} \cdot v \cdot \mathrm{d}t}{\int v \cdot \mathrm{d}t}, \tag{3}$$

where P is the rate of penetration, m/rad, v is the advance rate of the shield machine, m/s, ω is the cutterhead rotation speed, rad/s, and T is the cutterhead torque, N·m.

To estimate the ATPI of the next ring, the current ring tunnel should be divided into M equal sections. Then, the ATPI of these sections is used as the original data for the ATPI prediction.

Finally, a wavelet-based GM(1,1) (WGM(1,1)) is designed for cutterhead load characteristic prediction. For forecasting the ATPI of the next ring, WGM(1,1) will firstly intercept a certain number of the latest sections' ATPI of current ring with a sliding window. Next, WGM(1,1) will obtain the main features of the ATPI data through wavelet transform. Based on the preprocessed ATPI, WGM(1,1) will forecast the ATPI of the sections along next ring through a grey model GM(1,1). Eventually, the predicted ATPI of the next ring can be calculated by averaging these sections' ATPI.

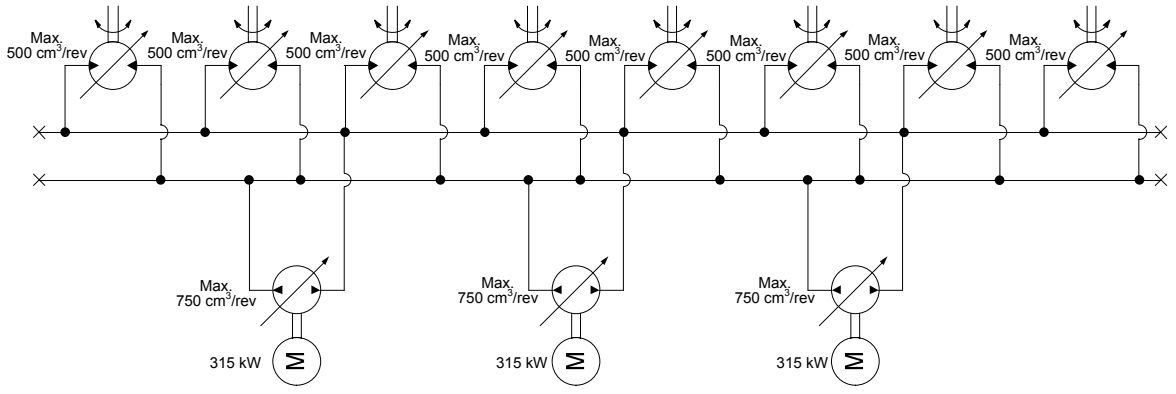

Fig. 2 A simplified cutterhead hydraulic driving system of CTE6250 (Xing *et al*., 2010)

The sliding window used for getting the latest ATPI data can be expressed as

$$\boldsymbol{F}(N)=\left[f(M-N+1), f(M-N+2), \cdots, f(i), \cdots, f(M)\right], \tag{4}$$

where i is the number of the current ring's section (i=1, 2, …, M), $f(i)$ is the ATPI of section i , and N is the number of data needed for prediction ($N \leq M$).

2.1 Wavelet-based preprocessing

Wavelet transform is a new time-frequency analysis approach. It can concentrate the general part of a signal in a small number of large coefficients. Based on this, a wavelet threshold filter is introduced to extract the main features of the field ATPI before prediction, which will be helpful in smoothing fluctuations and enhancing the precision of the prediction.

A method proposed by Mallat (1989) is used to perform the wavelet decomposition and reconstruction of signal (Li *et al*., 1995; Wang *et al*., 2007). The decomposition formula is

$$\begin{aligned} \overline{v}^{i+1}(n) &= \sum_k \overline{h}(2n-k)\,\overline{v}^{i}(k), \\ \overline{w}^{i+1}(n) &= \sum_k \overline{g}(2n-k)\,\overline{v}^{i}(k), \end{aligned} \tag{5}$$

where $\overline{v}^{i+1}(n)$ and $\overline{w}^{i+1}(n)$ are the scale coefficient and detail coefficient at the i+1 decomposition level, respectively, the initial coefficients $\overline{v}^{0}(n)$ can be defined as input signal $\boldsymbol{F}(N)$, and $\overline{h}(n)$ and $\overline{g}(n)$ are the decomposition filter banks. The reconstruction formula is

$$\tilde{v}^{i}(n)=\sum_k [\tilde{h}(2k-n)\cdot\tilde{v}^{i+1}(k)+\tilde{g}(2k-n)\cdot\tilde{w}^{i+1}(k)], \tag{6}$$

where $\tilde{v}^{i+1}(n)$ and $\tilde{w}^{i+1}(n)$ are the processed scale coefficient and detail coefficient at the i+1 decomposition level, respectively, and $\tilde{h}(n)$ and $\tilde{g}(n)$ are the reconstruction filter banks.

The 'noise' wavelet coefficients should be removed between wavelet decomposition and wavelet reconstruction. In each decomposition level, a soft thresholding method is used for 'noise' removal (Donoho, 1994; Postalcioglu, 2005)

$$\tilde{w}^{i}=\begin{cases} \operatorname{sign}(\overline{w}^{i})\cdot(\left|\overline{w}^{i}\right|-\lambda), & \left|\overline{w}^{i}\right|\geq\lambda, \\ 0, & \left|\overline{w}^{i}\right|<\lambda, \end{cases} \tag{7}$$

where λ is a threshold value which should be determined according to current geologic conditions.

2.2 Grey model GM(1,1)

The GM(1,1) model is a first-order one variable grey model which has been widely used in prediction. It can simulate system evolution tendencies through matching the regularity of previous observations. Thus, it is very suitable for a system without a valid mathematic model. The GM(1,1) algorithm (Deng, 1989; Hsu *et al*., 2003; Lin *et al*., 2011) is briefly described as follows:

Preprocessed data sequence to be analyzed,

$$\hat{\boldsymbol{F}}(N)=x^{(0)}=\{x^{(0)}(1), x^{(0)}(2), \cdots, x^{(0)}(N)\}. \tag{8}$$

Accumulated generating operation (AGO) is used to reveal the internal discipline,

$$x^{(1)}=\left\{\sum_{i=1}^{1}x^{(0)}(i), \sum_{i=1}^{2}x^{(0)}(i), \sum_{i=1}^{3}x^{(0)}(i), \cdots, \sum_{i=1}^{N}x^{(0)}(i)\right\}. \tag{9}$$

A first-order differential equation is used to model the AGO data,

$$\frac{\mathrm{d}x^{(1)}(t)}{\mathrm{d}t}+a\cdot x^{(1)}(t)=b, \tag{10}$$

where a is the developing coefficient, and b is the grey input.

With the help of the least square method, we can obtain:

$$\begin{bmatrix} a \\ b \end{bmatrix}=(\boldsymbol{B}^{\mathrm{T}}\boldsymbol{B})^{-1}\boldsymbol{B}^{\mathrm{T}}\boldsymbol{Y}, \tag{11}$$

where

$$\boldsymbol{B}=\begin{bmatrix} -\frac{1}{2}(x^{(1)}(1)+x^{(1)}(2)) & 1 \\ -\frac{1}{2}(x^{(1)}(2)+x^{(1)}(3)) & 1 \\ \vdots & \vdots \\ -\frac{1}{2}(x^{(1)}(N-1)+x^{(1)}(N)) & 1 \end{bmatrix}, \quad (12)$$

$$\boldsymbol{Y}=\begin{bmatrix} x^{(0)}(2) & x^{(0)}(3) & x^{(0)}(4) & \cdots & x^{(0)}(N) \end{bmatrix}^{\mathrm{T}}. \quad (13)$$

Solving the differential equation, we can obtain the fitted sequence of AGO data,

$$\hat{x}^{(1)}(j)=(x^{(0)}(1)-b/a)\times \mathrm{e}^{-a(j-1)}+b/a. \quad (14)$$

Inverse accumulated generating operation (IAGO) is applied to obtain the fitted sequence of the original data

$$\hat{x}^{(0)}(j)=(x^{(0)}(1)-b/a)(1-\mathrm{e}^{a})\times \mathrm{e}^{-a(j-1)}. \quad (15)$$

Then, we can obtain the predicted ATPI of the ith section of the next ring

$$\hat{x}^{(0)}(N+i)=(x^{(0)}(1)-b/a)(1-\mathrm{e}^{a})\times \mathrm{e}^{-a(N+i-1)}, \quad (16)$$

where $1\leq i\leq M$.

To solve the singular problem caused by $a\to 0$, L'hopital's rule is used (Chen *et al*., 2013)

$$\hat{x}^{(0)}(N+i)=\begin{cases}(x^{(0)}(1)-b/a)(1-\mathrm{e}^{a})\times \mathrm{e}^{-a(N+i-1)}, & |a|>\varepsilon, \\ b, & |a|\leq\varepsilon, \end{cases} \quad (17)$$

where ε is a small threshold value.

Finally, the predicted ATPI of the next ring can be calculated by averaging the M predicted ATPI of the next ring's sections.

$$\overrightarrow{\mathrm{ATPI}}=\mathrm{average}(\hat{x}^{(0)}(N+1),\hat{x}^{(0)}(N+2),\cdots,\hat{x}^{(0)}(N+M)). \quad (18)$$

2.3 Numerical analysis

In this study, the field data for analysis was collected from the tunnel between the Houting and Songgang stations on the No. 11 line of the Shenzhen Metro. The tunnel was constructed using a CTE6250 machine. The machine can gather and save field data once every second. The field data of rings No. 49 to No. 250 were used for prediction and analysis.

For comparison, both GM(1,1) and WGM(1,1) were used for ATPI prediction. The forecasted ATPI of rings No. 50 to No. 250 are shown in Fig. 3. WGM(1,1) first obtains the overall trend and then forecasts the ATPI. In contrast, GM(1,1) forecasts directly according to the field section's ATPI. But local fluctuations in the field section's ATPI can mislead the forecasting of GM(1,1). Therefore, compared with WGM(1,1), the outcome of GM(1,1) shows greater fluctuation.

To investigate and compare the accuracy of the two models, the mean relative error (MRE) was introduced (Hsu *et al*., 2003):

$$\mathrm{MRE}=\frac{1}{m}\sum_{k=1}^{m}\left|\frac{\mathrm{ATPI}(k)-\overrightarrow{\mathrm{ATPI}(k)}}{\mathrm{ATPI}(k)}\right|, \quad (19)$$

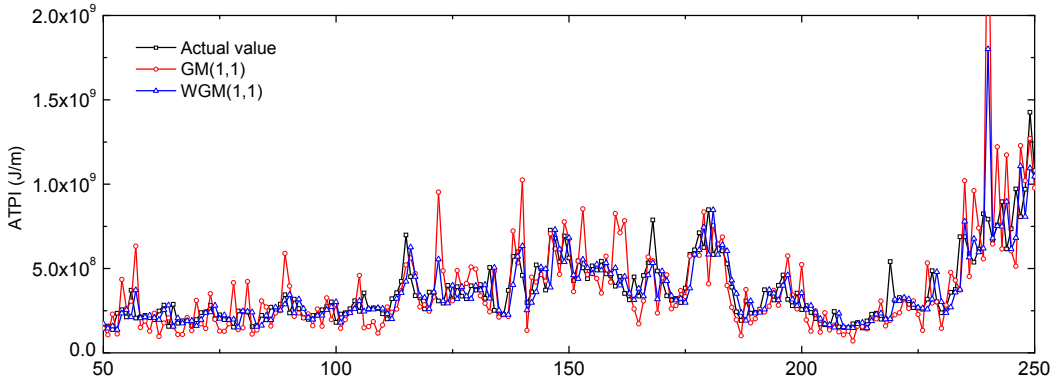

Fig. 3 Forecasted ATPI using GM(1,1) and WGM(1,1) with M=8, N=8

where m is the number of the rings, ATPI(k) is the ATPI of ring k, and $\overrightarrow{\text{ATPI}(k)}$ is the predicted ATPI of ring k.

Table 1 summarizes the prediction performance of the two models, under different sliding window size N and section count of one ring M. WGM(1,1) achieved a good prediction accuracy, better than that of GM(1,1). Therefore, wavelet transform preprocessing can help the GM(1,1) model improve prediction performance. The wavelet-based GM(1,1) model is an effective way to forecast the cutterhead load characteristic.

Table 1 Forecast errors of GM(1,1) and WGM(1,1), m=201

Model	MRE				
	N=4		N=8		
	M=4	M=8	M=8	M=12	M=16
GM(1,1)	34.7%	63.5%	34.0%	39.8%	56.8%
WGM(1,1)	20.8%	19.6%	20.1%	19.5%	19.7%

3 Cutterhead efficiency optimization

The cutterhead load characteristic fluctuates widely along the tunnel (Fig. 3). The cutterhead driving hydraulic system needs to have sufficient power to deal with possible heavy loads. However, the cutterhead load may also be very low. Such light-load conditions will lead to a reduction in motor efficiency.

3.1 Change of stator winding connection

The change of stator winding connection (delta connection or star connection) is a simple and effective method to improve motor efficiency. In the case of a heavy load, the stator winding will be a delta connection. If the load is below a specific value, it changes from a delta (D) connection to a star (Y) connection (Ferreira *et al*., 2005; Ferreira and de Almeida, 2006). The specific load value is the intersection between the D connection efficiency curve and the Y connection efficiency curve, as shown in Fig. 4 (Ferreira and de Almeida, 2006; Ferreira, 2009).

3.2 Cutterhead mode control strategy (CMCS)

Based on both the WGM(1,1) and the change of stator winding connection, a cutterhead mode control strategy (CMCS) was developed (Fig. 5). Whenever one ring of excavation is done, the WGM(1,1) model will firstly be used to forecast the ATPI of the next ring. Based on the predicted ATPI, an advance rate maximum (ARM) formula is applied to provide a recommended advance speed range (0–v_{ARM}). This speed range will help the operator to set a reasonable advance rate. After receiving the advance rate order and predicted ATPI, a rotation speed minimum (RSM) formula is used to provide a recommended cutterhead speed range (n_{RSM}–n_{MAX}). Again, this speed range will help the operator to set a reasonable rotation speed. The advance rate order and predicted

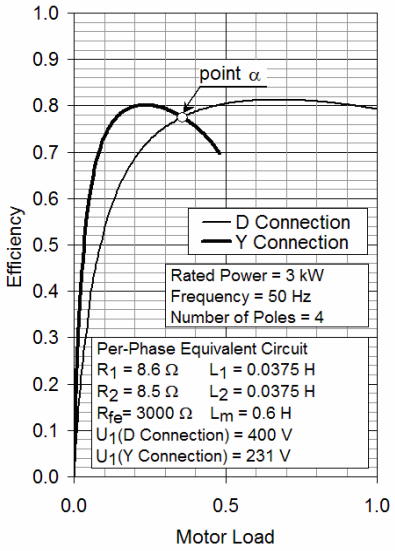

Fig. 4 Simulated motor efficiency (Reprinted from (Ferreira and de Almeida, 2006), Copyright 2006, with permission from IEEE)

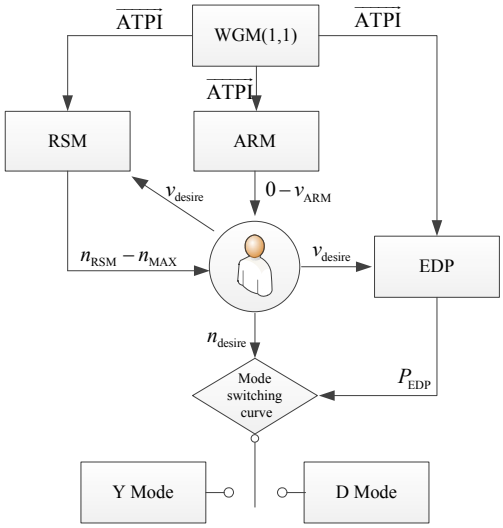

Fig. 5 Cutterhead mode control strategy

ATPI are also put into an estimated driving power (EDP) formula to estimate the driving power of the next ring (P_{EDP}). Finally, both the rotation speed order and P_{EDP} are used to decide the reasonable mode according to preset mode switching points.

The ARM formula is

$$v_{ARM}=\frac{P_{rate}\cdot\eta_e}{\overrightarrow{ATPI}\cdot\eta_s}, \tag{20}$$

where P_{rate} is the total rated power of the three cutterhead motors, η_e is the transfer efficiency of the cutterhead driving system, and η_s is a safety factor to prevent overload caused by forecast and load nonlinear errors.

The RSM formula is

$$n_{RSM}=\frac{\overrightarrow{ATPI}\cdot\eta_s\cdot v_{desire}}{T_{rate}}, \tag{21}$$

where v_{desire} is the advance rate order from the operator, and T_{rate} is the rated torque of cutterhead.

The EDP formula is

$$P_{EDP}=\overrightarrow{ATPI}\cdot\eta_s\cdot v_{desire}. \tag{22}$$

4 Experiments and discussion

4.1 Experimental platform

To test the energy-saving performance of our proposed strategy, the strategy was applied to an experimental platform. The platform consists mainly of a driving system and a torque loading system (Fig. 6). The driving system is a typical pump controlled motor system (installed power 30 kW) driven by a Y/D switching circuit. The torque-loading system provided a simulated cutterhead torque load for the driving system. The input power, output torque, output speed and some other state parameters of the driving system could be sampled and saved in real time.

4.2 Mode switching curve

On this platform, a contrast test was implemented between the D and Y connections (Fig. 7). The Y connection mode had a better energy efficient performance under a light load, but the D connection mode performed better under a heavy load. The turning point in energy efficient performance can be easily calculated from the intersection of the two efficiency curves.

During excavation, the cutterhead speed needs to be adjusted to cope with the load conditions and to

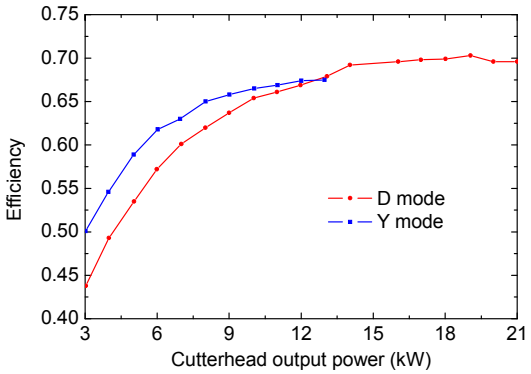

Fig. 7 System efficiency as a function of cutterhead output power, with a controlled cutterhead speed of 1200 r/min

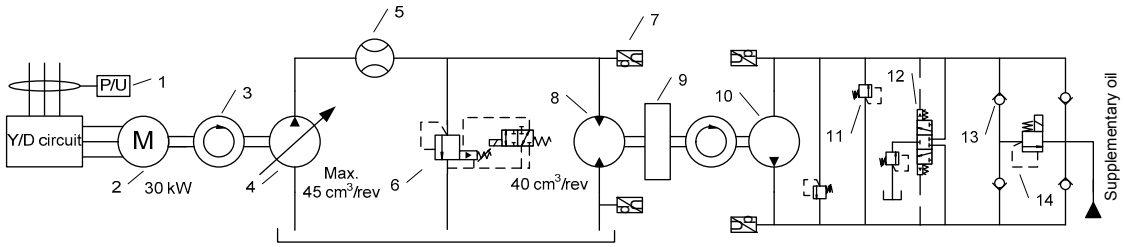

1: power sensor; 2: three-phase asynchronous motor; 3: torque & speed sensor; 4: variable pump; 5: flow sensor; 6: electromagnetic relief valve; 7: pressure sensor: 8: fixed displacement motor; 9: inertia load; 10: fixed displacement pump; 11: relief valve; 12: pilot operated direction valve; 13: check valve; 14: proportional relief valve

Fig. 6 Experimental platform for simulating the shield cutterhead driving system

cooperate with other subsystems. Therefore, more contrast tests were carried out at different cutterhead speeds (Fig. 8). The preset mode switching points should be the crossing points of the efficiency curves, under different cutterhead speeds. Based on the measured switching points, we could obtain a mode switching curve for the simulated cutterhead driving system.

4.3 Numerical analysis and experiments

To further investigate the performance of the CMCS, numerical analysis and experiments based on field data were carried out. Firstly, field data of rings 60, 110, 160, and 210 were selected as the subject in this study. Then, numerical analysis was carried out according to the CMCS (Table 2).

Because the field data were not the field response of the CMCS, the v_{desire} was set as the mean value of the actual advance rate v_{mean} and the n_{desire} was set as the mean value of the actual cutterhead rotation speed n_{mean}. To apply the calculation results to the experimental platform, the following transformations were then carried out.

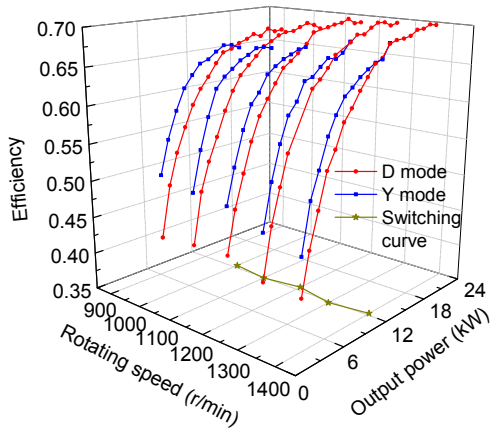

Fig. 8 Efficiency and switching points, with different controlled cutterhead speeds

$$n_{\text{EPdesire}} = \lambda_{\text{n}} n_{\text{desire}},\ P_{\text{EPEDP}} = \lambda_{\text{P}} P_{\text{EDP}}, \tag{24}$$

where n_{EPdesrie} is the desired rotation speed for the experimental platform, λ_{n} and λ_{P} are the speed similarity coefficient and power similarity coefficient between the experimental platform and the cutterhead driving system, respectively, and P_{EPEDP} is the estimated output power for the experimental platform.

Based on the desired rotation speed, estimated output power, and mode switching curve, the mode was decided. Finally, experiments were carried out based on the mode output of the CMCS. To apply the field data to the experimental platform, the following transformation was carried out:

$$n_{\text{EP}} = \lambda_{\text{n}} n,\ T_{\text{EP}} = \lambda_{\text{T}} T, \tag{25}$$

where n_{EP} is the transformed rotation speed, n is the field cutterhead rotation speed, T_{EP} is the transformed torque, λ_{T} is the torque similarity coefficient between the experimental platform and the cutterhead driving system, and T is the field cutterhead torque. After transformation, every third data point was sampled as an instruction for the experiment and the time interval between each instruction was set to 0.4 s to accelerate the progress of the experiment. Fig. 9 shows the results of the experiment. To verify better energy efficiency of the CMCS, contrast tests were also conducted. From the comparison, we can see that the CMCS consumes less power under a light load.

A further energy consumption investigation was carried out (Table 3). For each experiment, we could obtain the total energy by integrating the motor input power. Then, we could obtain the efficiency. According to the results, it is clear that the CMCS can improve system efficiency.

Table 2 Numerical computing results of the CMCS with $\eta_{\text{e}} = 0.6$, $\eta_{\text{s}} = 1.3$, $\lambda_{\text{n}} = 807.4$, and $\lambda_{\text{P}} = 3.17\times10^{-2}$

Ring No.	CTE6250						Experiment platform		
	Forecasted ATPI ($\times10^5$ kJ/m)	v_{ARM} ($\times10^{-3}$ m/s)	Assume $v_{\text{desire}}=v_{\text{mean}}$ ($\times10^{-3}$ m/s)	P_{EDP} ($\times10^2$ kW)	n_{RSM} ($\times10^{-2}$ rad/s)	Assume $n_{\text{desire}}=n_{\text{mean}}$ ($\times10^{-2}$ rad/s)	P_{EPEDP} (kW)	n_{EPdesire} (rad/s)	Mode
60	2.23	1.96	0.79	2.29	3.82	15.9	7.26	128	Y
110	2.63	1.66	0.87	2.97	4.96	15.8	9.41	128	Y
160	5.04	0.87	0.85	5.57	9.28	15.5	17.66	125	D
210	1.50	2.91	1.03	2.01	3.35	15.7	6.37	127	Y

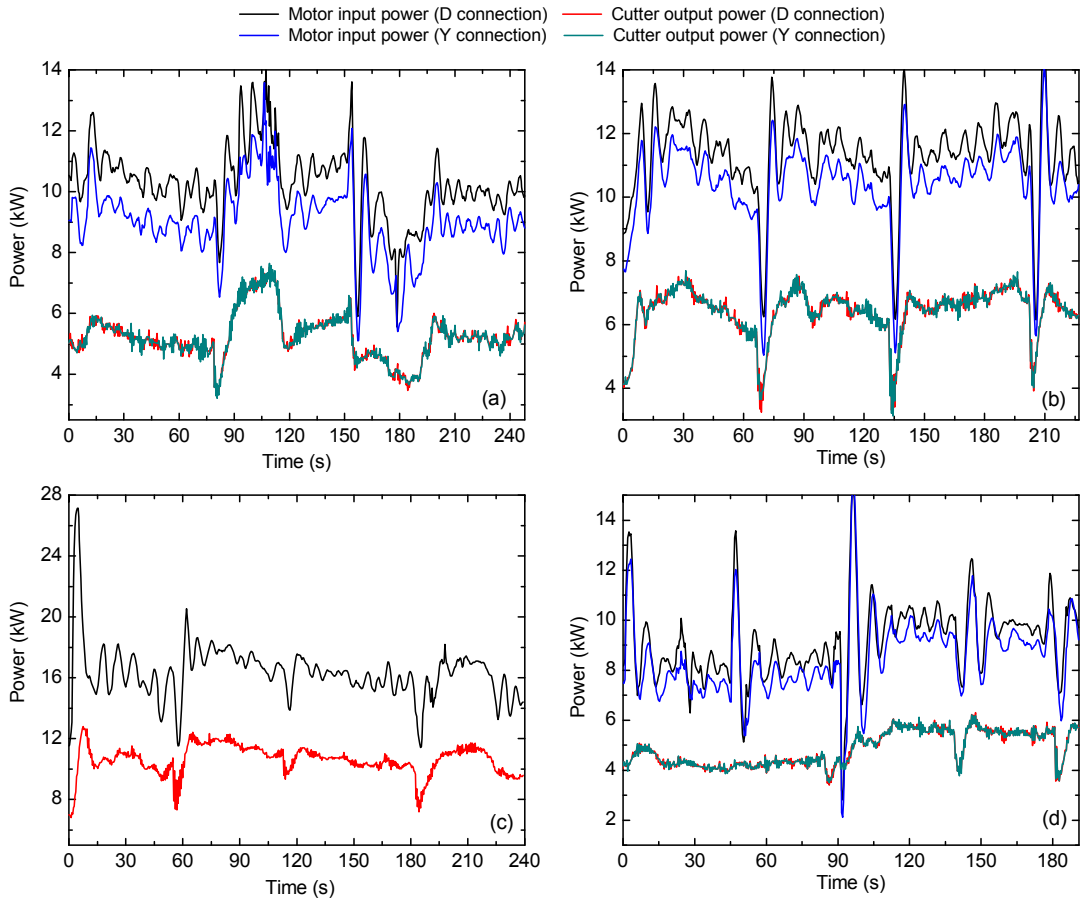

Fig. 9 Experiments based on field data
(a) Ring No. 60; (b) Ring No. 110; (c) Ring No. 160; (d) Ring No. 210

Table 3 Experiment results analysis

Approach	Ring No. 60		Ring No. 110		Ring No. 160		Ring No. 210	
	Output (kJ)	Efficiency (%)	Output (kJ)	Efficiency (%)	Output (kJ)	Efficiency (%)	Output (kJ)	Efficiency (%)
Without CMCS	1300	51.0	1458	56.6	2542	64.9	928	53.0
With CMCS	1301	57.8	1458	61.5	2542	64.9	928	57.0

5 Conclusions

In this paper, we propose a mode control strategy for a shield cutterhead hydraulic driving system based on a load characteristic forecast method. The following conclusions can be drawn:

1. The wavelet transform preprocessing can help the GM(1,1) to improve performance in forecasting the cutterhead load characteristic. The WGM(1,1) is an effective method for forecasting the cutterhead load characteristic.

2. The change of stator winding connection is a simple and efficient technique to improve the efficiency of cutterhead hydraulic system.

3. The CMCS can provide the operator with recommendations about the advance rate range and cutterhead rotation speed range, which will be helpful in developing a reasonable construction plan for the next ring. The stator winding connection can also be optimized according to the construction plan. Consequently, CMCS has shown a satisfactory energy-saving performance in the field data-based experiments.

References

Chen, C.I., Huang, S.J., 2013. The necessary and sufficient condition for GM (1,1) grey prediction model. *Applied Mathematics and Computation*, **219**(11):6152-6162. [doi:10.1016/j.amc.2012.12.015]

Donoho, D.L., Johnstone I.M., 1994. Threshold selection for wavelet shrinkage of noisy data. Proceedings of the 16th Annual International Conference Engineering in Medicine and Biology Society, **1**:A24-A25. [doi:10.1109/IEMBS.1994.412133]

Deng, J.L., 1989. Introduction to grey system theory. *The Journal of Grey System*, **1**(1):1-24.

Ferreira, F.J.T.E., 2009. Strategies to Improve the Performance of Three-phase Induction Motor Driven Systems. PhD Thesis, University of Coimbra, Portugal.

Ferreira, F.J.T.E., de Almeida, A.T., 2006. Method for in-field evaluation of the stator winding connection of three-phase induction motors to maximize efficiency and power factor. *IEEE Transactions on Energy Conversion*, **21**(2):370-379. [doi:10.1109/TEC.2006.874248]

Ferreira, F.J.T.E., de Almeida, A.T., Ge, B.M., *et al.*, 2005. Automatic change of the stator-winding connection of variable-load three-phase induction motors to improve the efficiency and power factor. IEEE International Conference on Industrial Technology, Hong Kong, China. [doi:10.1109/ICIT.2005.1600842]

He, C., Feng, K., Fang, Y., *et al*., 2012. Surface settlement caused by twin-parallel shield tunnelling in sandy cobble strata. *Journal of Zhejiang University-SCIENCE A (Applied Physics & Engineering)*, **13**(11):858-869. [doi:10.1631/jzus.A12ISGT6]

Hsu, C.C., Chen, C.Y., 2003. Applications of improved grey prediction model for power demand forecasting. *Energy Conversion and Management*, **44**(14):2241-2249. [doi:10. 1016/S0196-8904(02)00248-0]

Li, H., Manjunath, B.S., Mitra, S.K., 1995. Multisensor image fusion using the wavelet transform. *Graphical Models and Image Processing*, **57**(3):235-245. [doi:10.1006/gmip.1995.1022]

Lin, C.S., Liou, F.M., Huang, C.P., 2011. Grey forecasting model for CO_2 emissions: a Taiwan study. *Applied Energy*, **88**(11):3816-3820. [doi:10.1016/j.apenergy.2011.05.013]

Liu, X.Y., Yuan, D.J., 2014. An *in-situ* slurry fracturing test for slurry shield tunneling. *Journal of Zhejiang University-SCIENCE A (Applied Physics & Engineering)*, **15**(7):465-481. [doi:10.1631/jzus.A1400028]

Mallat, S.G., 1989. A theory for multiresolution signal decomposition: the wavelet representation. *IEEE Transactions on Pattern Analysis and Machine Intelligence*, **11**(7):674-693. [doi:10.1109/34.192463]

Postalcioglu, S., Erkan, K., Bolat, E.D., 2005. Comparison of Kalman filter and wavelet filter for denoising. International Conference on Neural Networks and Brain, **2**:951-954. [doi: 10.1109/ICNNB.2005.1614777]

Shi, H., Yang, H.Y., Gong, G.F., *et al.*, 2014. Energy saving of cutterhead hydraulic drive system of shield tunneling machine. *Automation in Construction*, **37**:11-21. [doi:10.1016/j.autcon.2013.09.002]

Song, K.Z., Sun, M., 2007. Analysis of influencing factors of shield tunneling performance in complex rock strata. *Chinese Journal of Rock Mechanics and Engineering*, **26**(10):2092-2096 (in Chinese).

Wang, S.N., Pan, Y.H., Yang, J.G., 2007. Study on spillover effect of copper futures between LME and SHFE using wavelet multiresolution analysis. *Journal of Zhejiang University-SCIENCE A*, **8**(8):1290-1295. [doi:10.1631/jzus.2007.A1290]

Xing, T., Yang, H.Y., Gong, G.F., 2009. Drive technique of pumps optimized combination hydraulic system in shield tunneling machine. *Journal of Zhejiang University (Engineering Science)*, **43**(3):511-516 (in Chinese). [doi:10.3785/j.issn.1008-973X.2009.03.022]

Xing, T., Yang, H.Y., Gong, G.F., 2010. Efficiency comparative study for hydraulic drive system of cutter head in shield tunneling machine. *Journal of Zhejiang University (Engineering Science)*, **44**(2):358-363, 372 (in Chinese). [doi:10.3785/j.issn.1008-973X.2010.02.027]

Yang, H.Y., Xing, T., Gong, G.F., 2010. Variable speed pump control system for driving cutterhead of test shield tunneling machine. *Journal of Zhejiang University (Engineering Science)*, **44**(2):373-378 (in Chinese). [doi:10.3785/j.issn.1008-973X.2010.02.030]

Zhang, Q., 2012. Mechanics Characteristic Analysis and Modeling for Load of Shield Machine during Tunneling. PhD Thesis, Tianjin University, China (in Chinese).

中文概要

题　目： 一种基于载荷特征预测的盾构机刀盘节能驱动技术

目　的： 实现盾构机刀盘载荷特征预测，并将预测结果应用于刀盘驱动系统的能耗优化控制。

方　法： 1. 采用基于小波变换的灰色模型 WGM(1,1)对盾构机刀盘载荷特征进行预测；2. 基于该预测方法，设计刀盘模式控制策略（CMCS），实现刀盘驱动系统的能耗优化控制。

结　论： 1. 相对传统灰色模型 GM(1,1)，基于小波变换的灰色模型 WGM(1,1)可更加精确地预测盾构机刀盘载荷特征，是一种更加有效的载荷特征预测方法；2. 改变电动机定子接线方式是一种简单有效的提升刀盘系统效率的方法；3. 刀盘模式控制策略不仅可以为操作者提供操作建议，而且可以通过优化电机定子接线方式，降低刀盘在低载荷下的能量消耗，提升刀盘驱动系统的效率。

关键词： 盾构机刀盘；驱动系统；载荷特征预测；刀盘模式控制策略（CMCS）